Efficient Image Registration with Subpixel Accuracy using a Hybrid Fourier-based Approach

Jelina Unger and Klaus Brinker
Hamm-Lippstadt University of Applied Sciences, Marker Allee 76-78, 59063 Hamm, Germany

Keywords: Image Registration, Fourier-based Cross Correlation, Image Projections, Subpixel Accuracy.

Abstract: In many fields like medical imaging and remote sensing, it is necessary to register images with subpixel accuracy. A general problem is the tradeoff between accuracy and efficiency. This paper presents a highly accurate and efficient algorithm for subpixel image registration using Fourier-based cross correlation to determine the translation between two images. Therefore a coarse to fine strategy is used. It combines a fast method using image projections with an accurate approach using matrix multiplication for refined computation. The results show that the new approach has almost the same level of accuracy as the accurate method, but with reduced computational complexity. Compared to the fast method, the computational complexity of the new approach is slightly higher, but achievs a higher level of accuracy. Overall the hybrid approach achieves an efficient registration with a relatively short runtime.

1 INTRODUCTION

Image registration is the process of aligning two or more images of the same object on top of each other. For this purpose the transformation between those images is determined. Typical transformation types are rotation, scaling, and translation. In this paper we focus on translations which is suitable, e.g. for microscopic applications among others. Many applications require calculation of the transformation down to a fraction of a pixel, i.e. with subpixel accuracy. In medical imaging, this allows monitoring changes in the human body of one patient but also facilitates comparing different patients. For this purpose images of different times or modalities are registered (Farncombe and Iniewski, 2014).

Fourier-based methods have gained increasing attention in recent years. The basic method is to compute an upsampled version of the cross correlation between two images using the discrete Fourier Transform (DFT) and locate its peak. In general, the main problem is to exhibit high accuracy and low computational time simultaneously (Tong et al., 2019). Guizar-Sicairos et al. (2008) present a highly accurate approach. A coarse to fine strategy is implemented using matrix multiplication to be more efficient. Still, this approach yields a high computational complexity. A fast approach is presented by Yang et al. (2012). They only use image projections which reduces the runtime but also decreases the level of accuracy. The aim of the present work is to combine both approaches to one highly efficient and accurate hybrid algorithm.

Section 2 presents the basic methods of Fourier-based image registration and outlines the three algorithms. In Section 3, an evaluation of the algorithms and different relevant influencing factors are presented. The results are discussed in Section 4. Finally a conclusion is given in Section 5.

2 REGISTRATION METHODS

In the following, we first introduce the definitions of the DFT, explain the basic method for subpixel image registration, and lastly present the three algorithms.

The DFT and its inverse can be calculated by different methods. In this paper the transformation formula and matrix multiplication are used. The transformation formula for 1D-DFT of a signal *f(x)* with length *N* is shown in Equation 1 (McAndrew, 2016).

$$F(u) = \sum_{x=0}^{N-1} f(x) \exp\left\{-2\pi i \frac{xu}{N}\right\} \qquad (1)$$

The inverse 1D-DFT of the Fourier-Spectral *F(u)* can be calculated using Equation 2.

$$f(x) = \frac{1}{N} \sum_{u=0}^{N-1} F(u) \exp\left\{2\pi i \frac{xu}{N}\right\} \qquad (2)$$

Images can be described as a two-dimensional function *F(x,y)* with dimensions $N \times M$. Therefore, the

Unger, J. and Brinker, K.
Efficient Image Registration with Subpixel Accuracy using a Hybrid Fourier-based Approach.
DOI: 10.5220/0010242901360143
In *Proceedings of the 14th International Joint Conference on Biomedical Engineering Systems and Technologies (BIOSTEC 2021) - Volume 2: BIOIMAGING*, pages 136-143
ISBN: 978-989-758-490-9

generalized 2D-DFT formula is necessary, which is shown in Equation 3.

$$F(u,v)=\sum_{x=0}^{N-1}\sum_{y=0}^{M-1} f(x,y)\exp\left\{-2\pi i\left(\frac{ux}{N}+\frac{vy}{M}\right)\right\} \tag{3}$$

The inverse 2D-DFT is calculated by Equation 4.

$$f(x,y)=\frac{1}{MN}\sum_{u=0}^{N-1}\sum_{v=0}^{M-1} F(u,v)\exp\left\{2\pi i\left(\frac{xu}{N}+\frac{yv}{M}\right)\right\} \tag{4}$$

Matrix multiplication is another method to calculate the (inverse) 2D-DFT of images (Soummer et al., 2007). It can be expressed as

$$F(u,v)=w_{XU}\cdot f(x,y)\cdot w_{YV} \tag{5}$$

and

$$f(x,y)=\frac{1}{N}w^*_{XU}\cdot F(u,v)\cdot\frac{1}{M}w^*_{YV} \tag{6}$$

where w_{XU} and w_{YV} are the transformation matrices and * indicates the complex conjugation. They are defined by Equation 7 and 8.

$$w_{XU}=\exp\{-2\pi iXU\} \tag{7}$$

$$w_{YV}=\exp\{-2\pi iYV\} \tag{8}$$

The vectors X and U are defined as

$$X=\begin{cases}[0,1,...,N-1]-\frac{N}{2} & \text{for even N}\\ [0,1,...,N-1]-\frac{N-1}{2} & \text{for odd N}\end{cases} \tag{9}$$

and

$$U=\begin{cases}\frac{1}{N}\cdot[0,1,...,\frac{N}{2}-1,-\frac{N}{2},...,-1] & \text{for even N}\\ \frac{1}{N}\cdot[0,1,...,\frac{N-1}{2},-\frac{N-1}{2},...,-1] & \text{for odd N}\end{cases} \tag{10}$$

where N describes the height of the image. Y and V are computed analogously but with the exception that image width M replaces height N.

2.1 Subpixel Image Registration

In general, the translation between two images *f(x,y)* and *g(x,y)* can be described as

$$f(x,y)=g(x-\Delta x,y-\Delta y) \tag{11}$$

where Δx and Δy are the vertical and the horizontal shifts (Tong et al., 2019). We define f as the reference image and g as the image to be registered. To compute these translations, Fourier-based cross correlation is computed by Equation 12 and its peak has to be located (Anuta, 1970).

$$CC(x,y)=\mathcal{F}^{-1}(F(u,v)G^*(u,v)) \tag{12}$$

G and F denote the Fourier-Transform of images g and f, * indicates the complex conjugation and $\mathcal{F}^{-1}$ the inverse DFT. For achieving subpixel accuracy, an upsampled version of the cross correlation is required. Therefore, the number of data points is increased by a factor of κ, allowing a theoredical accuracy of $\frac{1}{\kappa}$ of a pixel. A common method to achieve upsampling is zero-padding (Shin et al., 2017). For this, the product $F(u,v)G^*(u,v)$ with size $N\times M$ is embedded in a larger array of zeros with size $\kappa N\times\kappa M$. Calculating the inverse DFT of this array results in an upsampled version of the cross correlation. Finally the peaks are located and the shifts are converted to the original pixel units (Yang et al., 2012).

Another method to perform upsampling is to calculate the inverse DFT by using matrix multiplication. For this, the transformation matrices must be adjusted by increasing the value range of the vectors X, Y, U and V by the upsampling factor κ. Furthermore, the upsampling can be limited to a specific image region. The vector X is computed by

$$X=\begin{cases}[0,1,...,D\kappa-1]-\frac{D\kappa}{2}+s\kappa & \text{for even D}\kappa\\ [0,1,...,D\kappa-1]-\frac{D\kappa-1}{2}+s\kappa & \text{for odd D}\kappa\end{cases} \tag{13}$$

where D denotes the image region height and s the vertical center. Y is computed analogously with the exception that the width replaces the height and the horizontal replaces the vertical center. To calculate the vector U Equation 14 is used.

$$U=\begin{cases}\frac{1}{\kappa N}\cdot[0,1,...,\frac{N}{2}-1,-\frac{N}{2},...,-1] & \text{for even N}\\ \frac{1}{\kappa N}\cdot[0,1,...,\frac{N-1}{2},-\frac{N-1}{2},...,-1] & \text{for odd N}\end{cases} \tag{14}$$

To compute V, the same approach can be used by replacing the height N with the width M (Soummer et al., 2007).

Due to the increase of data points, the upsampling is always related to a higher computational complexity. The advantage of the matrix multiplication is that the upsampling can be localized to a specific image region (Tong et al., 2019).

2.2 Matrix Multiplication DFT Approach

A highly accurate algorithm to register images by using Fourier-based cross correlation is presented by Guizar-Sicairos et al. (2008). A coarse to fine strategy is used. The first step is to compute the Fourier-based cross correlation over the entire image using zero-padding with an upsampling factor of $\kappa_0=2$ and to locate its peak. In the second step, an upsampled version of the 1.5×1.5 pixel neighborhood around the rough estimation is computed by matrix multiplication. At this point the upsampling factor is adjustable. The peak is located in the output array and converted into units of original pixels. The last step is to combine the rough and refined estimation to the final translation vector. We refer to this algorithm as MM.

2.3 Image Projections DFT Approach

A high-speed algorithm for subpixel image registration is presented by Yang et al. (2012). To reduce computational time, one-dimensional image projections are used to compute the upsampled Fourier-based cross correlations.

First, vertical and horizontal image projections are calculated by taking the sum of each row respectively column, using Equation 15 and 16 for an image *f(x,y)* with height *N* and width *M*.

$$f_{row}(x) = \sum_{y=0}^{M-1} f(x,y) \qquad (15)$$

$$f_{col}(y) = \sum_{x=0}^{N-1} f(x,y) \qquad (16)$$

The information of edges can influence the cross correlation. To reduce this effect a filter is applied, which is shown in Equation 17 and 18.

$$f_{row,filt}(x) = f_{row}(x) - \left[\frac{1}{N}\sum_{i=0}^{N-1} f_{row}(i)\right] \qquad (17)$$

$$f_{col,filt}(y) = f_{col}(y) - \left[\frac{1}{M}\sum_{j=0}^{M-1} f_{col}(j)\right] \qquad (18)$$

This preprocessing step is performed for both images *f(x,y)* and *g(x,y)*. All filtered projections are transformed in the frequency domain by using the transformation formula. Hence, two products $F_{row}(u)G^*_{row}(u)$ and $F_{col}(v)G^*_{col}(v)$ are computed. In order to achieve subpixel accuracy, zero-padding is used. For this purpose both products are embedded in larger arrays of zeros with size κN respectively κM. Computing the inverse 1D-DFT with the transformation formula of these arrays results in upsampled versions of cross correlations. Finally peaks are located and converted into units of original pixels to receive vertical and horizontal translations. We refer to this algorithm as IP.

2.4 Combination of Image Projections and Matrix Multiplication DFT

In this paper we present a novel efficient algorithm which combines the MM algorithm from (Guizar-Sicairos et al., 2008) and the IP algorithm from (Yang et al., 2012). The main idea is to keep the high accuracy of MM, but with low computational time like IP. Therefore, we consider a coarse to fine strategy. For the first rough estimation, the IP approach is used with an upsampling factor of $\kappa_0 = 2$. MM is used for the refined estimation of translation. A more detailed computational process visualization is given in Figure 1 and explained in the following. This steps are performed for two images *f(x,y)* and *g(x,y)*:

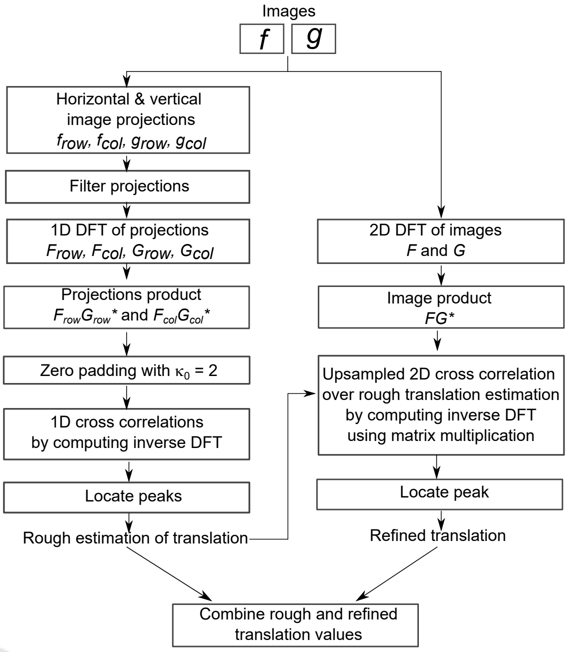
Images
f
g
Horizontal & vertical image projections $f_{row}, f_{col}, g_{row}, g_{col}$
Filter projections
1D DFT of projections $F_{row}, F_{col}, G_{row}, G_{col}$
Projections product $F_{row}G_{row}{}^*$ and $F_{col}G_{col}{}^*$
Zero padding with $\kappa_0 = 2$
1D cross correlations by computing inverse DFT
Locate peaks
Rough estimation of translation
2D DFT of images F and G
Image product FG^*
Upsampled 2D cross correlation over rough translation estimation by computing inverse DFT using matrix multiplication
Locate peak
Refined translation
Combine rough and refined translation values

Figure 1: Computational process of the proposed combination approach.

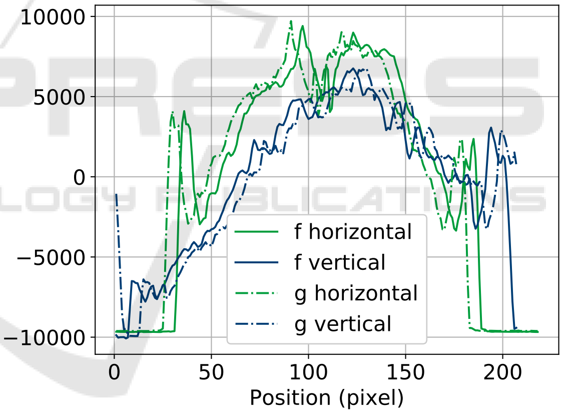

Figure 2: Filtered image projections for the reference image *f* and the image to be registered *g*.

1. Rough shift estimation
   (a) compute and filter vertical and horizontal projections of both images
   (b) compute upsampled Fourier-based cross correlations of vertical and horizontal projections

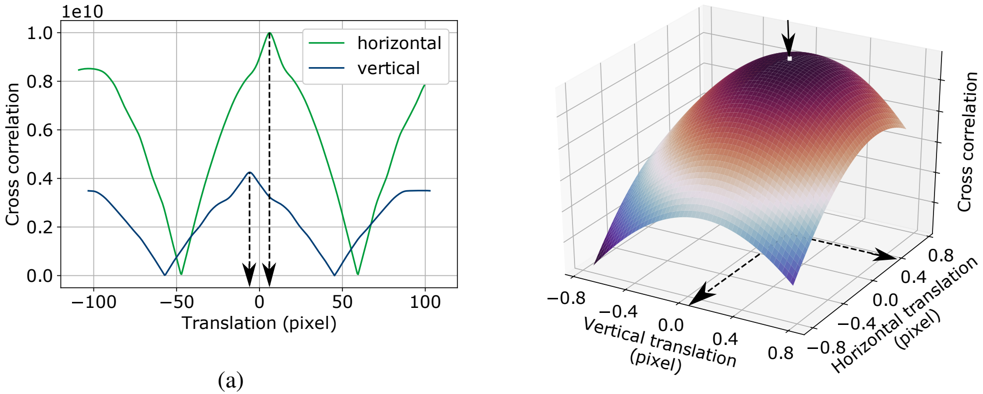

(a)

(b)

Figure 3: Visualization for the main steps of combination algorithm: (a) 1D rough cross correlations and (b) 2D refined cross correlation around the rough estimation, where the locations of peaks are marked by arrows.

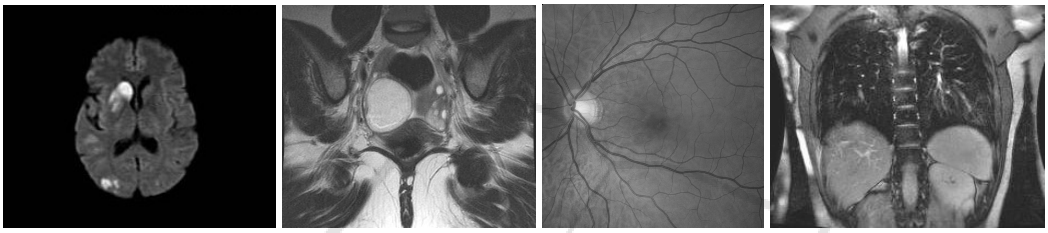

Figure 4: Four examples of test images from (He et al., 2020), (Budai et al., 2013) and (Cohen, 2020).

with an upsampling factor of $\kappa_0 = 2$ by using zero-padding and transformation formula

(c) locate the peak and convert it into original pixel units

2. Refined shift estimation

   (a) compute the product $F(u,v)G^*(u,v)$ and define transformation matrices w_{XU} and w_{YV} for image region centered over the rough estimated peak with a region size of $1.5\kappa \times 1.5\kappa$ pixel in upsampled pixel units

   (b) compute the upsampled cross correlation by multiplying these three matrices

   (c) locate the peak and convert into original pixel units

3. Add rough and refined estimation for receiving the total translation vector

The filtered image projections are visualized in Figure 2. It can be seen that projections of the image g have the same shape as the reference image f, but are shifted slightly. Figure 3 shows the cross correlations for the first rough and the refined estimation. The rough estimation consists of two one-dimensional cross correlations for the vertical and horizontal direction. Their peaks can clearly be determined for -6 and 6 pixels. The refined cross correlation over the rough estimation has a peak at $(0.32, 0.10)$. For both cross correlation plots, peaks and their corresponding position are marked by arrows. In total a translation of $(-5.68, 6.10)$ is determined for this sample image pair by adding rough and refined estimation.

2.5 Implementation

All three algorithms were implemented in Python (version 3.7.1). Standard libraries especially NumPy (version 1.18.1) and its modul numpy.fft for discrete Fourier Transform were used. The library Scikit-image (version 0.16.2) was only used for loading images. For the MM approach the implementations from (Guizar, 2016) and (Fezzani et al., 2020) were used. Evaluation is performed on a HP 250 G5 Notebook with Intel(R) Core Processor 2.40 GHz, 8 GB RAM and 64-bit-operating-system.

3 EVALUATION

In this section, we evaluate all three algorithms with respect to accuracy and runtime. First, the methods for conducting the evaluation are described. Further on, the general performance for accuracy and runtime is evaluated. Additionally, we analyze performance for different image sizes and under the presence of

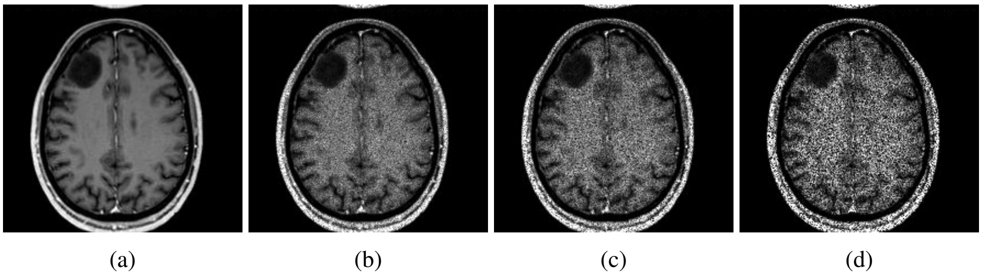

Figure 5: Visualization of different noise variances for a test image (He et al., 2020): (a) 0, (b) 0.05 (c) 0.1 and (d) 0.3.

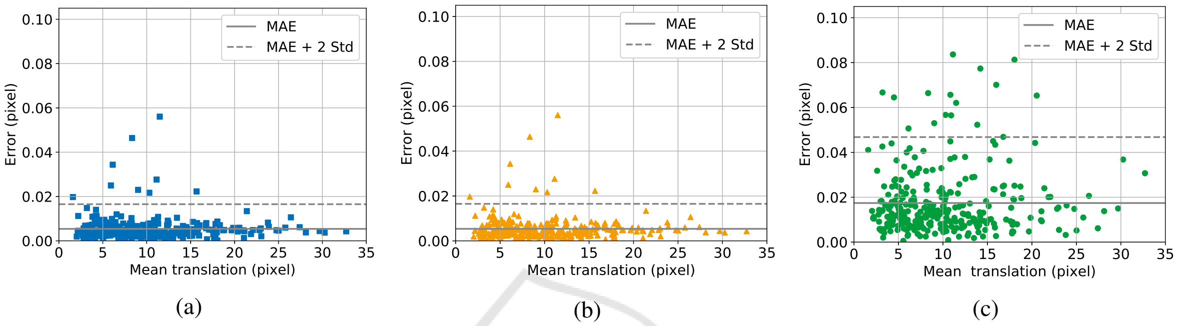

Figure 6: Visualization of the pixel error versus mean translation for (a) MM, (b) combination algorithm and (c) IP.

noise. The final part of the evaluation includes an analysis of the influence of different upsampling factors.

3.1 Methods

For the evaluation, a dataset of 300 medical images from (He et al., 2020), (Budai et al., 2013) and (Cohen, 2020) is used for the reference images. Four sample images are shown in Figure 4. In order to obtain an image to be registered for each reference image, a random translation is performed which is between 0.5 % and 3 % of the corresponding image side. Additionally, noise is added to slightly change the image information in contrast to the reference image.

To evaluate the accuracy, the mean value is calculated from the absolute vertical and horizontal error for each image pair. Additionally, the mean absolute error (MAE) is calculated over the entire dataset in order to assess general performance. Furthermore, the runtime is measured and the mean value is calculated over the dataset to evaluate the efficiency. The tolerances are given by the doubled standard deviation (Std).

For the first three parts of evaluation, an upsampling factor of $\kappa = 100$ is used. In order to analyze the performance with noisy images, the dataset is extended. The same translations as for the first three parts are used, but six images to be registered with different noise levels for every reference image are created. A multiplicative Gaussian noise is used. The noisy image is defined as $image_{noise} = image + n * image$, where n is Gaussian noise with zero mean and different variances in the range of 0 to 0.3. In Figure 5, four noise levels are shown by a sample test image.

3.2 General Performance

The results for the general performance of all algorithms are shown in Table 1. The MM and combination algorithm have the same high level of accuracy of 0.005 ± 0.011 pixel for the MAE. The MAE of the IP approach is more than three times as large. But the IP method has the shortest runtime with 0.019 ± 0.029 s. The combination algorithm is just slightly slower, but MM requires significantly more time. Accordingly, the combination algorithm reduces the MAE in contrast to the IP approach by over 70 % and runtime in contrast to the MM approach by over 75 %.

Table 1: General performance for all algorithms.

Algorithm	**MAE (pixel)**	**Runtime (s)**
MM	0.005 ± 0.011	0.324 ± 0.562
Combination	0.005 ± 0.011	0.079 ± 0.125
IP	0.017 ± 0.029	0.019 ± 0.029

The results for the error in dependence on translation are visualized in Figure 6. Besides, the MAE the limit of tolerance for the dataset is given. It is shown that most error samples for MM and combina-

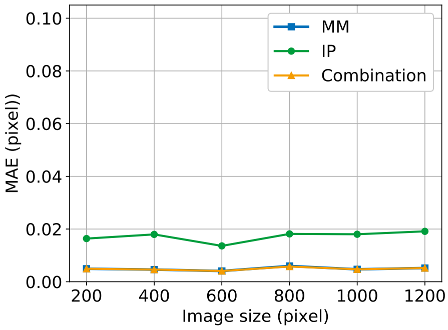

Figure 7: MAE depending on image size.

tion are within this limit. For the IP, the tolerance limit is larger and error samples spread more. Furthermore, the error is equally distributed over the translation size for all algorithms, therefore, no dependence between error and size of translation is visible here.

3.3 Dependency on Image Size

In the following, we analyze whether image size influences accuracy and runtime. To visualize accuracy, the images were grouped by size and the MAE were calculated for each group (Figure 7). As already shown in Section 3.2, the MAE for the IP approach is clearly higher than for the other two algorithms. The MAE for the MM and combination approach is exactly the same. However, for all algorithms the MAE is about the same for all sizes. There are only minor fluctuations that don't indicate a clear trend. Hence, no dependency can be determined.

Though, a clear dependency on the image size for the runtime can be determined, which is shown in Figure 8. The runtime increases with larger image size. For small images around 200 pixel image dimension, all algorithms have a low runtime under 0.04 s. But the runtime of the MM approach is already slightly higher. Additionally it shows the sharpest increase with a quadratic trend up to 1.2 s. The runtime of the combination approach also shows a quadratic trend, but the curve progression is much flatter though, reaching a maximum of only 0.26 s which is almost 80 % less than the MM. The IP approach shows only a slight linear increase in time up to 0.045 s.

3.4 Dependency on Noise

In the following we analyze the performance for images with different noise levels. Figure 9 shows the MAE at different noise levels. The MM and combination approach achieve low MAE. The MM approach has a slight linear increase of the MAE from 0.005 up to 0.015 pixel. For low noise levels the combination algorithm has the same accuracy as MM. Though starting from the noise variance of 0.1, the MAE increases slightly more up to 0.03 pixel. In contrast, the MAE of IP already rises steeply for low noise levels from 0.009 to 0.106 pixel. For the highest noise level, the MAE of the combination algorithm is twice as large as of the MM, but still 70 % less than of the IP approach.

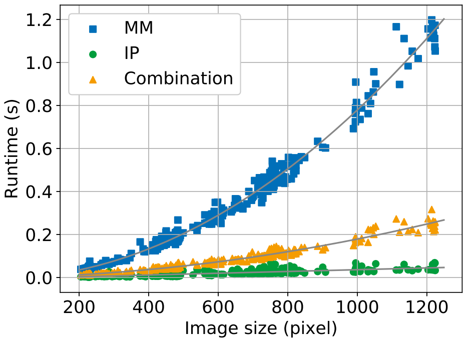

Figure 8: Runtime depending on image size.

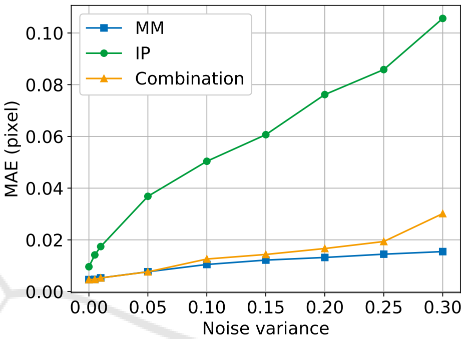

Figure 9: MAE depending on noise variance.

Table 2: MAE for general performance and noisy images.

Algorithm	MAE (pixel)	
	normal images	**noisy images**
MM	0.005 ± 0.011	0.010 ± 0.018
Combination	0.005 ± 0.011	0.013 ± 0.052
IP	0.017 ± 0.029	0.051 ± 0.172

In comparison to the general performance, which is presented in Section 3.2, the MAE of subpixel accuracy increases for all algorithms (Table 2). For MM and combination the MAE doubles, but for the combination the increase is slightly more. For the IP a steep increase can be observed. Moreover, the MAE is tripled. For normal images the error of the combination algorithm is 70 % less compared to IP and even 75 % for noisy images.

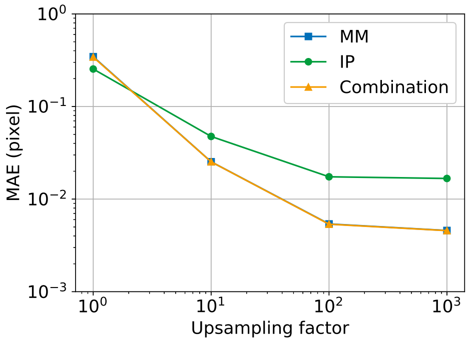

Figure 10: MAE depending on upsampling factor.

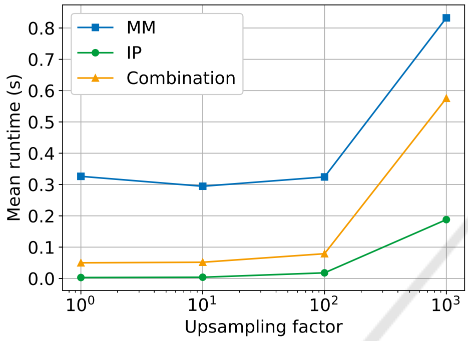

Figure 11: Runtime depending on upsampling factor.

3.5 Dependency on the Upsampling Factor

In the following, the influence of different upsampling factors to subpixel accuracy and runtime is evaluated. If the upsampling factor is increased by a factor of 10, the registration is theoretically more accurate by a factor of 10. However, Figure 10 shows that this is not always the case. For the IP, the decrease of MAE becomes less and from upsampling factor 100 to 1000 it totally stagnates. The MAE for MM and combination is exactly the same. In the beginning it decreases almost by a factor of 10. But for $\kappa = 1000$ it also stagnates.

At values of $\kappa = 1$, which means there is no upsampling, IP is slightly more accurate. But for higher values, the MAE of MM and the combination approach is significantly less. For the $\kappa = 10$, it is already 20 % and for $\kappa = 100$ and $\kappa = 1000$ it is more than 70 %.

Taking runtime into account, it can be observed that there are only slight changes for the first three upsampling factors 1 to 100, but for the highest factor runtime increases rapidly (Figure 11). Generally, the IP approach has the shortest runtime with 0.008 ± 0.03 s for an upsampling with the factor 1 to 100 and increases by 0.18 s for the highest factor. The MM approach has a considerably longer runtime with 0.315 ± 0.648 s for lower upsampling factors and increases more rapidly for the highest upsampling by 0.517 s. The runtime for the combination algorithm is slightly higher than for the IP, but significantly lower than for the MM with 0.060 ± 0.126 s for the lower upsampling factors. Though it increases by 0.516 s for the highest upsampling as the MM approach.

4 DISCUSSION

The purpose of this paper was to combine two image registration algorithms so that the translation between images can be determined with high accuracy and low computational requirements. The results have shown that our combination algorithm fulfills these two criteria. The MM approach is always the most accurate one, but the combination algorithm achieves almost the same level of accuracy. In contrast, the IP has always a significantly higher error. However, regarding runtime it is the most efficient. The combination algorithm can't achieve the same low runtime, but it is still in a very low range of a few milliseconds. Especially compared to the MM approach, runtime can be reduced significantly. Additionally, the combination algorithm isn't as sensitive to large image sizes. As seen in Figure 8, the runtime of the combination increases significantly less than for the MM approach. Hence, the dependency on the image size is low and therefore it is applicable to scenarios with large image dimensions.

We conclude that accuracy of all algorithms doesn't depend on translation and image size. As we only conducted limited experiments regarding the image and translation size, it can not be ruled out that the accuracy is dependent on translations, especially large ones. Because the larger the translation, the smaller the matching image regions. Thus, the similarity between both images is reduced, which could complicate the registration process. However as such large translation are rare in medicine, we choose this setting.

Guizar-Sicairos et al. (2008) states that the MM approach is robust to noise, because the whole image information is used for the rough estimation and all data points from the upsampled cross correlation as well. Our results confirm these findings as seen in Figure 9. The IP doesn't use the whole image information, because due to image projections the data is reduced. Hence, it is highly sensitive to noise. The combination algorithm is to a similar degree as MM robust to noise. Just for high noise levels it is slightly more sensitive. Conducting the first rough estimation by the projection method is mostly accurate enough.

If the real peak is still within proximity to the first estimation, the refined estimation can still recover it. If the rough estimation is very imprecise, an unavoidable error will occur in the refined determination. To improve the algorithm in this respect, the rough estimation can be refined by using a higher upsampling factor or to enlarge image region for the refined estimation. For this reason, it must be clarified whether the gain in accuracy is worth the increase in runtime.

The upsampling factor is a tool to achieve higher accuracy. For a factor κ translation can be determined by $\frac{1}{\kappa}$ of a pixel. Results have shown that this factor is limited to 100. Higher factors don't achieve higher accuracy. Additionally, a higher upsampling results in a longer runtime, because there are more data points to be processed. For low factors the increase in runtime isn't significant, because it's just a slight increase of data. However, for large factors like 1000 runtime increases rapidly. This property was observed for all algorithms. Finally an upsampling factor of $\kappa = 100$ is a suitable choice, because best accuracy can be achieved without rapid increase of runtime.

The combination algorithm is limited to determine translation between images. Therefore, our evaluation only focuses on paraxial translation between images. For most image registration problems, rotation and scaling has to be considered as additional transformations between images. In order to generalize our algorithm it can be extended to determine also other transformations: The Fourier-Mellin-Transformation can be used for computing rotation and scaling, and afterwards determining the translation (Tong et al., 2019).

5 CONCLUSIONS

This paper presents an efficient algorithm for image registration with subpixel accuracy. More precisely, we propose a hybrid approach consisting of a coarse to fine strategy. For the first rough estimation image projections are used, while for the refined estimation the method of matrix multiplication is performed only on a small region around the first estimation center. Experimental results have shown that the algorithm is very accurate and computationally highly efficient. The MAE can be reduced by over 70 % compared to the IP approach and runtime by over 75 % compared to the MM approach. It is robust with respect to noise and can handle large images. To improve the algorithm in further work, it can be extended to consider generalized transformation models, such as including rotation and scaling.

REFERENCES

Anuta, P. (1970). Spatial registration of multispectral and multitemporal digital imagery using fast fourier transform techniques. *IEEE Transactions on Geoscience Electronics*, 8(4):353–368.

Budai, A., Bock, R., Maier, A., Hornegger, J., and Michelson, G. (2013). Robust vessel segmentation in fundus images: High-resolution fundus image dataset. *International Journal of Biomedical Imaging*.

Cohen, J. (2020). Covid chest x-ray dataset. Available: https://github.com/ieee8023/covid-chestxray-dataset. (visited on July 22, 2020).

Farncombe, T. and Iniewski, K. (2014). *Medical imaging: Technology and applications*. Devices, circuits, and systems. CRC Press, Boca Raton, Fla.

Fezzani, R., Nunez-Iglesias, J., Lee, G. R., and Boulogne, F. (2020). scikit-image _phase_cross_correlation. Available: https://github.com/scikit-image/scikit-image/blob/v0.17.2/skimage/registration/_phase _cross_correlation.py. (visited on August 08, 2020).

Guizar, M. (2016). Effizient subpixel image registration by cross-correlation. Available: https://www.mathworks.com/matlabcentral/fileexchange/18401-efficient-subpixel-image-registration-by-cross-correlation. (visited on August 08, 2020).

Guizar-Sicairos, M., Thurman, S. T., and Fienup, J. R. (2008). Efficient subpixel image registration algorithms. *Optics letters*, 33(2):156–158.

He, X., Zhang, Y., Mou, L., Xing, E., and Xie, P. (2020). Pathvqa: 30000+ questions for medical visual question answering: Medical dataset. *arXiv preprint arXiv:2003.10286*.

McAndrew, A. (2016). *A computational introduction to digital image processing*. CRC Press, Boca Raton, FL, second edition.

Shin, J. G., Kim, J. W., Lee, J. H., and Lee, B. H. (2017). Accurate reconstruction of digital holography using frequency domain zero padding. In Chung, Y., Jin, W., Lee, B., Canning, J., Nakamura, K., and Yuan, L., editors, *25th International Conference on Optical Fiber Sensors*, SPIE Proceedings, page 103235H. SPIE.

Soummer, R., Pueyo, L., Sivaramakrishnan, A., and Vanderbei, R. J. (2007). Fast computation of lyot-style coronagraph propagation. *Optics express*, 15(24):15935–15951.

Tong, X., Luan, K., Stilla, U., Ye, Z., Xu, Y., Gao, S., Xie, H., Du, Q., Liu, S., Xu, X., and Liu, S. (2019). Image registration with fourier-based image correlation: A comprehensive review of developments and applications. *IEEE Journal of Selected Topics in Applied Earth Observations and Remote Sensing*, 12(10):4062–4081.

Yang, Y., Zhilong, Z., Xin, X., and ZhaoLin, S. (2012). An upsampling approach to subpixel registration based on gray scale projection. In *2012 Third International Conference on Digital Manufacturing & Automation*, pages 210–213. IEEE.